Elsevier. Versión aceptada. Licencia creative Commons CC BY-NC-ND

Crystallisation of amorphous Al-Y-Ni-(Cu) alloys.

F.G. Cuevas[1], S. Lozano-Perez[2], R.M. Aranda[1], F. Ternero[3]

[1] Department of Chemical Engineering, Physical Chemistry and Materials Science, Escuela Técnica Superior de Ingeniería, University of Huelva, Campus El Carmen, Avda. Tres de marzo s/n, 21071 Huelva, Spain
[2] Department of Materials, University de Oxford, 16 Parks Road, Oxford OX1 3PH, UK
[3] Department of Materials Science and Engineering, Escuela Técnica Superior de Ingeniería, University of Sevilla, Avda. de los Descubrimientos s/n, 41092 Sevilla, Spain

Correspondence: F.G. Cuevas, fgcuevas@dqcm.uhu.es

Abstract.

The nanocrystallisation behaviour and subsequent intermetallics formation of an amorphous Al_{88}-Y_4-Ni_8 alloy has been studied. A 1 at% of Al or Ni was also substituted by Cu and its effect studied. Differential scanning calorimetry has been used to measure the thermal stability of these amorphous alloys. Transmission electron microscopy showed the smaller size of the nanocrystals obtained during primary crystallisation when Cu is added. Using three-dimensional atom probe, it has been checked that Cu is homogeneously distributed in the amorphous matrix, not contributing to a heterogeneous nucleation around Cu clusters during the formation of nanocrystals. Transmission electron microscopy and X-rays diffraction are used to study the controversial intermetallics occurrence at higher temperatures. The sequence and characteristics of the intermetallics appearing in these alloys were sensitive to the presence of Cu. The evolution of these intermetallics, up to 600 °C, has been studied. Findings are compared with previous studies.

Keywords: Amorphous materials; melt spinning; Al-Y-Ni alloy; crystallization

1. Introduction.

Heating a metal above its melting temperature, followed by a very quick cooling to room temperature, makes possible to retain the typical disordered atomic structure of the liquid state. The obtained material is usually known as a metallic glass [1, 2]. However, depending on the composition, different cooling rates are required. This makes composition selection and fabrication procedure key factors in these processes. The obtained glasses can show remarkable mechanical, electrical, magnetic or chemical properties, therefore becoming very interesting for engineering applications [3, 4].

Among the different possible compositions, aluminium-rich amorphous alloys have been intensively studied during the last decades. The main interest resides in their greater strengths with respect to conventional aluminium alloys [5], usually attributed to the absence of dislocations appearing in periodic crystalline lattices. Other interesting mechanical properties are their high elastic strain [6], or the possible presence of a supercooled liquid range allowing superplastic forming [7].

Achieving the current knowledge on the Al-base glassy materials has not been straight forward. The problems of brittleness found in the initial amorphous ribbons of ternary Al-Fe-X(B, Si, Ge) alloys [8, 9] were fixed by using Al-Ni-X(Si, Zr) compositions [10, 11]. Then, the studies of Al-RE(rare earth: La, Y, Ce)-TM(transition metal: Fe, Co, Ni) [12-16] resulted in higher strengths of up to about 1100 MPa.

It was also found that, for some alloys, the strength could be further increased by partial crystallisation of the amorphous phase to form a fine dispersion of α-Al nanocrystals [17]. Nanocrystals can represent a volume fraction up to 50% [18]. These amorphous-nanocrystalline alloys show the most desirable mechanical properties, even with improved ductility and toughness [19]. For the system Al-RE-Ni, values of 1100 and 1560 MPa [20, 21] have been reported for the amorphous and partially crystalline alloys respectively. These values are approximately two and three times higher than those in conventional crystalline aluminium alloys.

The high strength of nanocrystallised alloys has been attributed to different mechanisms. One of them is the increase of the shear slip resistance caused by the higher mechanical strength of primary α-Al nanocrystals with respect to the amorphous precursor areas [20]. In addition, the higher strength of the remaining amorphous matrix, due to solute enrichment after the formation of nanocrystals [22], or the influence of both the α-Al nanocrystals and the

remaining amorphous matrix [23], has been also considered. In any case, the microstructural characteristics (number density, size and distribution) of the nanocrystals play an important role on the properties of these materials. It is well known [17] that a better control of crystallisation is achieved by quenching to a fully amorphous state, and then partially devitrifying by a controlled annealing. On the other hand, it is also known that the crystallisation of intermetallics at higher temperatures produces a deleterious effect on the alloys properties [24].

One of the Al-RE-TM possible combinations, the Al-Y-Ni system, is studied here. According to previous results on kinetics of crystallisation and phase competition [18, 25-27], prediction of the glass forming range [28, 29], and modelling of the optimum amorphous forming composition [30, 31], the Al-rich corner of the ternary alloy with around a 10-15 at% of solute is a good glass former in this system. Thus, the Al_{88}-Y_4-Ni_8 alloy has been selected. Other well-known parameter affecting the glass forming ability (GFA) and the crystallisation process, the addition of small amounts of different alloying elements such as B, Cu, Be, Si, Ce, Mn, Fe or Co, among others, has been profusely studied in the Al-RE-Ni systems [32-38]. In particular, Cu addition has been proved to reduce the size of α-Al nanocrystals in different Al-RE-Ni systems [33, 39], improving mechanical properties after primary crystallisation, and will be here studied.

This work will not be limited to primary crystallisation, since one of the key objectives is still to obtain bulk amorphous alloys [2]. Several hundreds of different bulk metallic glasses (BMG) compositions have been discovered up to now, with recent studies, based on metallic glasses forming rules, predicting up to 3 million BMG alloys from 32 different elements (known to form metallic glasses and excluding rare earth and toxic elements) [40]. These rules can be based on the physical properties of the glass and competing crystalline phases, and can be as diverse as viscosity, fragility, density, liquidus temperature, glass transition temperature, crystallization temperature, structure and density of states of competing crystalline phases, or combinations of these properties as the known parameters S and g or the Turnbull criteria [40]. These properties are usually known once the glass is discovered, although new prediction techniques have been developed [41]. On the other hand, other properties such as the confusion principle based on the atomic size of the constituent elements, heats of mixing and electronegativities can also be used for predicting purposes. However, the GFA of Al-based alloys are not easily understood by the usually applied

criteria, and light-weight Al-based BMG are not easy to produce, being limited the production to relatively low Al contents [42]. Thus the Al-Y-Ni system is not a good candidate for BMG processing, and the option to easily obtain a bulk material has to involve processing the amorphous ribbon by powder metallurgy methods. In order to reach any of these goals, understanding the non-desirable high-temperature crystallisation stages is needed, particularly during forming processes of the obtained amorphous ribbons. For instance, spark plasma sintering has recently been applied to mechanically alloyed Al_{86}-Y_6-Ni_8 amorphous powders [43, 44], where temperatures of up to 400 ºC are necessary for consolidation.

2. Experimental procedure.

The alloy Al_{88}-Y_4-Ni_8 has been selected in this work. Substitution of Cu for Al or Ni, with compositions Al_{87}-Y_4-Ni_8-Cu_1 or Al_{88}-Y_4-Ni_7-Cu_1, have also been studied. For a better compositional control and lower melting temperatures during specimen preparation, pure metals (purity > 99.9 %) have been vacuum arc melted after Ti-gettering to obtain the Al_{90}-Cu_{10} and Al_{25}-Y_{75} master alloys. The required amount of these master alloys and the necessary pure metals have been arc melted again to obtain the final desired compositions. Ribbons have been obtained after melt spinning at 1000 ºC with a wheel surface velocity of 40 m/s, a nozzle-wheel distance of 1.5 mm and an ejection pressure of 50 mbar in a 200 mbar He atmosphere. Using a round nozzle of approximately 0.85 mm, ribbons with thicknesses of 25-30 μm and widths of 1-2 mm were obtained.

The microstructure of melt-spun, as well as of heat treated ribbons, was examined with X-rays diffraction (XRD, Philips PW 1729, with Cu-K_α radiation for 2θ = 20-80º) and transmission electron microscopy (TEM, Philips CM20 at 200 KV). For TEM studies, specimens were prepared by electropolishing in a solution of 10 % perchloric acid in 90 % ethanol, at –30 °C approximately. In some cases, to eliminate the effect of the preferentially attack of the Al nanocrystals in heat treated ribbons, electropolishing was followed by ion beam milling after cooling the specimens for 0.5 hours at –30 °C. A detailed examination of the spatial chemical distribution was carried out with a three-dimensional atom probe (3DAP) after primary

crystallisation, with special attention to the presence of Cu in the obtained microstructure.

Thermal stability studies and heat treatments of the ribbons were carried out in a differential scanning calorimeter (DSC, TA Instruments 2010) with a heating rate of 20 °C/min under an inert Ar atmosphere. Specimens were cooled inside the DSC cell after switching off the equipment.

3. Results and discussion.

3.1. Melt-spun ribbons

Figure 1 shows the XRD patterns of melt-spun ribbons for the different compositions studied. A broad peak at 2θ ~ 38º, characteristic of amorphous structures in Al alloys, can be observed in all the traces. A small shoulder in the amorphous halo, indicative of very small regions of local order [36, 45], appears for 2θ ~ 44º. For the studied compositions, this pseudo-peak can usually be detected in XRD patterns, but even smaller local order areas can be detected by nuclear magnetic resonance spectroscopy [26] or atom probe tomography [46], when not detected with XRD. This somewhat reduced GFA, not always found in Al-RE-Ni systems, could be due to the slightly lower difference between the atomic radius of Al and Y, with respect to other Al-RE pairs (with Sm, Gd, Nd, Ce, Pr, La) [47], therefore resulting in a lower GFA according to the confusion principle [48].

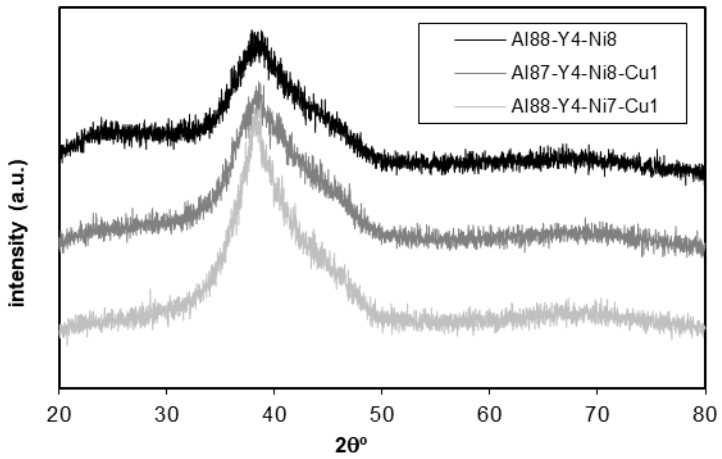

Figure 1. XRD patterns of melt-spun ribbons of the studied alloys.

The amorphous structure obtained after melt spinning is confirmed with TEM observations. A representative dark field (DF) micrograph is shown in

Figure 2, where some of the small white dots could correspond to local order areas.

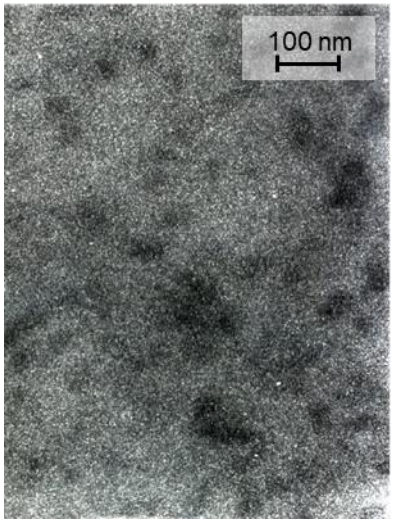

Figure 2. TEM dark field micrograph of the Al_{87}-Y_4-Ni_8-Cu_1 melt-spun ribbon.

3.2. Crystallisation process

Figure 3 shows the DSC traces for the melt-spun materials. The crystallisation process occurs in three stages, related to the different exothermic reactions appearing in the curves. As shown by several other researchers, this is the usual behaviour for the studied compositional range. However, crystallisation can be quite sensitive to composition. Thus, the commonly studied Al_{85}-Y_5-Ni_{10} [30, 36, 45, 49-51], Al_{86}-Y_4-Ni_{10} [52] or Al_{86}-Y_6-Ni_8 [53] alloys are reported to crystallize in the aforementioned three-stage mode, but the crystallisation of $Al_{88.5}$-$Y_{6.5}$-Ni_5 [54], Al_{85}-Y_4-Ni_{11} [18], Al_{83}-Y_4-Ni_{13} [52] or Al_{87}-Y_7-Ni_6 [47] has four stages. In addition, some studies only report two stages. It should be noted that the heating rate in DSC experiments does not only affect the transformations temperatures, but also the possibility of detecting them when appearing very close [37, 45, 55, 56]. Similarly, the use of synchrotron XRD revealed a two-stage crystallisation process in Al_{87}-Y_4-Ni_9 and Al_{86}-Y_4-Ni_{10}, but three stages for Al_{83}-Y_4-Ni_{13} [26].

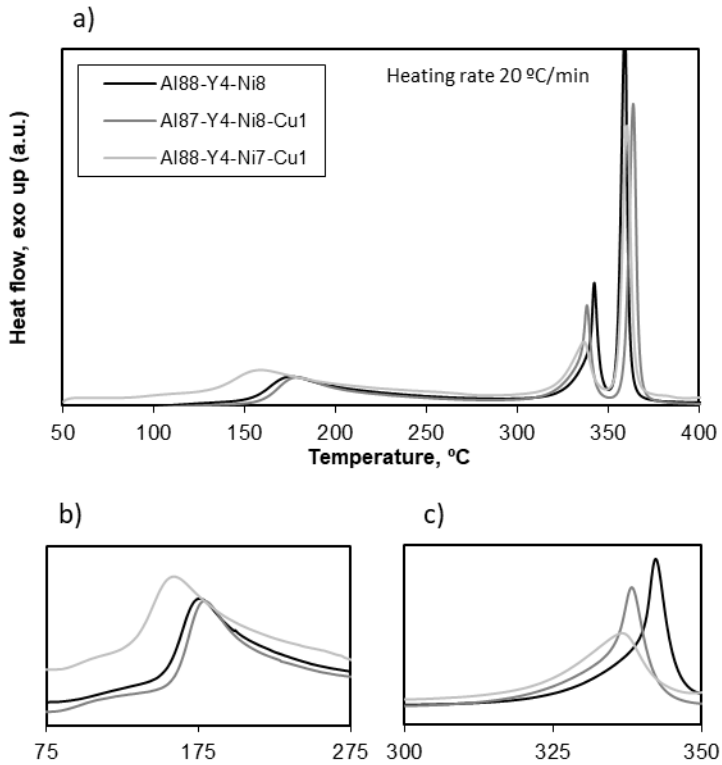

Figure 3. a) DSC traces of melt-spun ribbons of the studied alloys, and details of b) the first and c) the second crystallisation reactions.

3.3. Primary crystallisation

The first exothermic reaction in the crystallisation process (shown in detail in Figure 3b) is a broad one with the maximum at around 175 °C. A slightly more stable alloy results when 1 at% Cu replaces Al. Because of the increase in the amount of solute, and just considering the confusion principle [48] (other factors, such as the interaction force among atoms pairs, could also be considered), the reaction maximum is shifted to higher temperatures. On the other hand, when 1 at% Cu replaces Ni, the total amount of solute is the same, but the amorphous structure stability is clearly reduced. The atomic radius difference for Al-Cu is smaller than that of the pair Al-Ni. This can be explained by taking into account that the formation of an amorphous phase is less likely as the difference in atomic size gets smaller [57]. Thus, the first reaction is shifted to lower temperatures.

XRD studies on heat treated ribbons at the end of the first reaction show that this reaction is related to the formation of α-Al nanocrystals (Figure 4), apparently through a nucleation and growth mechanism [47, 58]. The lattice

parameter of the cubic α-Al crystals, measured from the peak positions in XRD patterns, is 0.4067 and 0.4095 nm for Cu-free and Cu-containing alloys, respectively. These values are higher than the 0.4050 nm of pure Al, indicating the preferential presence of alloying elements like Y in the solid solution. On the other hand, the smaller atomic radius of Y, when compared to other RE in Al-RE-Ni alloys, allows the rejected solute atoms to easily diffuse and not to accumulate around the just formed α-Al nanocrystals [47]. The primary crystallisation of intermetallic phases is thus avoided.

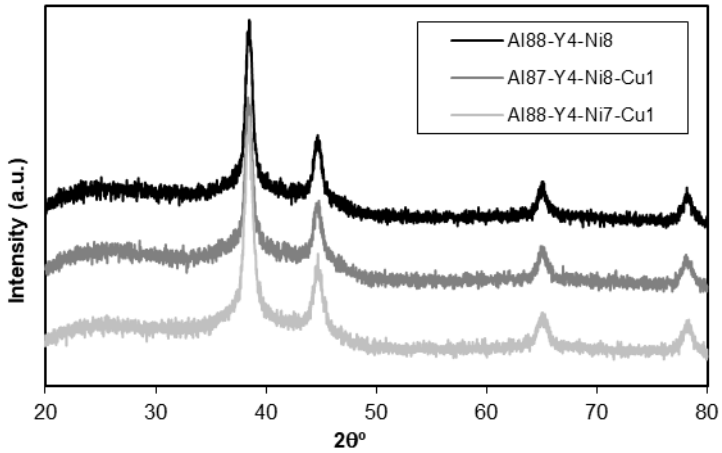

Figure 4. XRD patterns of ribbons of the studied alloys after heat treated to the end of the first DSC reaction. Observed peaks correspond to α-Al nanocrystals.

A detailed examination of the DSC traces (Figure 3b) shows that, before the primary crystallisation, there is a small exothermic reaction. Heat treating any of the alloys up to the formation of a fraction of the α-Al nanocrystals (for instance, heating up to the onset of the first reaction), and running new DSC experiments, makes this small exothermic reaction no longer to appear. On this basis, this pre-reaction could be related to the nucleation of most of the α-Al nanocrystals. An additionally observed phenomena in this pre-peak is the change of its onset temperature after ageing the ribbons at room temperature. Carrying out DSC experiments within 24 hours of the melt spinning process results in a pre-reaction onset temperature at approximately 80 °C for the three alloys. However, if DSC runs are carried out after a period of 200 days, it is displaced to 110 °C. Therefore, the nucleation process could slowly be taking place at room temperature. Figure 5 shows the difference between these two time-apart experiences for the Al_{87}-Y_4-Ni_8-Cu_1 alloy.

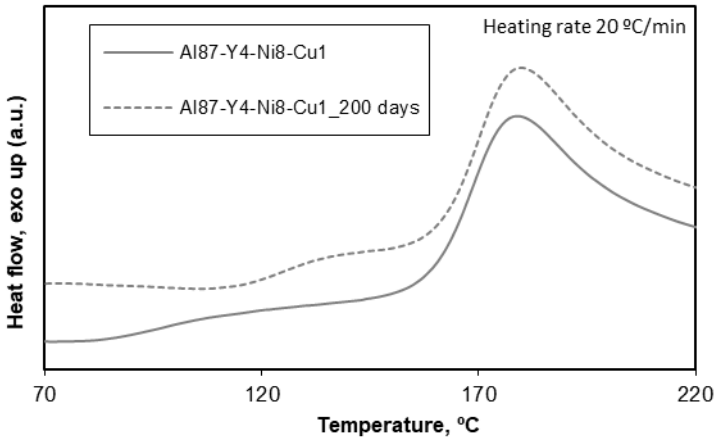

Figure 5. DSC traces of melt-spun ribbons of Al_{87}-Y_4-Ni_8-Cu_1 alloy carried out just after the melt spinning process and after 200 days.

Regarding the first DSC reaction, it is also worth noting that, for the studied compositions, a supercooled liquid region is not observed before primary crystallisation. Only some Al-Y-Ni alloys lead to both T_g and T_x, needing at least 10 at% of Y [37], although the alloys Al_{85}-Y_8-Ni_7 [38] and Al_{85}-Y_9-Ni_6 [47] have also been reported to show a glass transition temperature. When present, a relatively big supercooled liquid region is reported, contrarily to other Al-RE-Ni alloys, due to the small electronegativity difference between Al and Y [47].

Figure 6 shows the TEM microstructures observed after heat treatments at the maximum temperature of the first DSC reaction. Measurements on several micrographs, after checking that a similar volume fraction of nanocrystals had formed (calculated according to the area under the DSC curves), indicate that the addition of Cu reduces the size of nanocrystals. Crystals size mean values change from 9.8 nm in the Cu-free alloy, to 9.2 and 7.9 nm in Cu-substituting Al and Ni respectively, this is around a 6 and 20 % decrease.

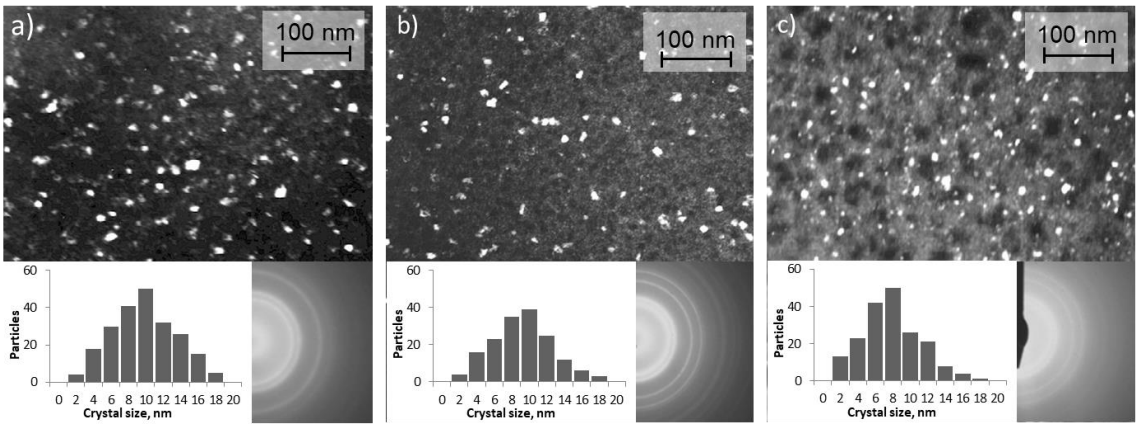

Figure 6. TEM dark field images and diffraction patterns (DP) of heat treated ribbons up to the maximum temperature of the first DSC reaction, and measured nanocrystals of a) Al_{88}-Y_4-Ni_8, b) Al_{87}-Y_4-Ni_8-Cu_1 and c) Al_{88}-Y_4-Ni_7-Cu_1 alloys.

Two possible mechanisms could be initially considered responsible for this size reduction. The first one is due to a growth limitation because of Cu segregation around just formed Al nuclei. In this case, diffusion mechanisms, atomic bonding strengths and interfacial effects should be considered responsible for this reduction. As a consequence of the smaller size, a higher number of nanocrystals should appear. The second mechanism to be considered is a reduction in size due to a direct increase in the number of nanocrystals. In this case, either a heterogeneous nucleation at Cu clusters or a reduction of the nucleation barrier for α-Al nanocrystals should be considered. The increased number of α-Al nanocrystals would then result on a size reduction. Among the previous mechanisms, clustering around Cu is known to operate in a Fe-based FINEMET alloy ($Fe_{73.5}$-$Si_{13.5}$-B_9-Nb_3-Cu_1), with Cu clusters acting as precursor sites for primary crystallisation of Fe nanocrystals [59].

In order to clarify the role of Cu on nanocrystals size, the Al_{88}-Y_4-Ni_7-Cu_1 alloy has been characterized by 3DAP (Figure 7) after been heat treated up to the end of the first DSC reaction.

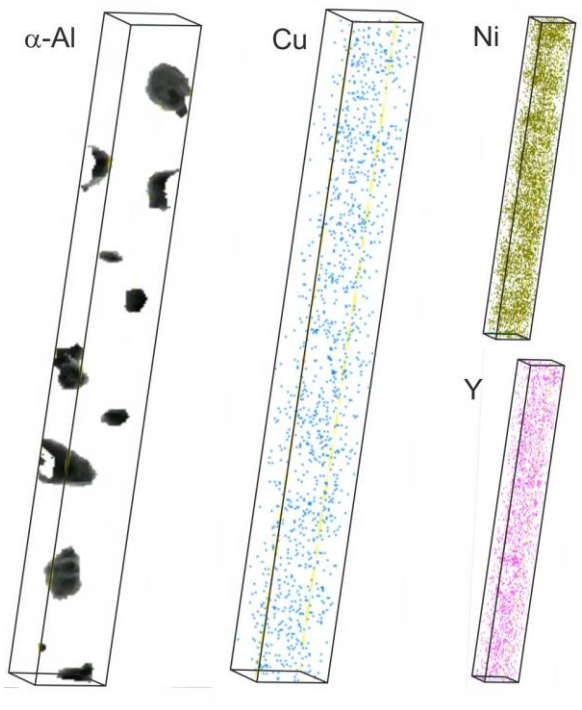

Figure 7. 3DAP results obtained from a volume of 11x11x100 nm^3 of an Al_{88}-Y_4-Ni_7-Cu_1 alloy heat treated up till the end of the first DSC reaction. α-Al isosurface of 96.5 at.% and elemental maps of Cu, Ni and Y are shown.

Cu is observed not to cluster, but to be homogeneously distributed in the remaining amorphous matrix. Therefore, neither the aforementioned growth limitation nor the heterogeneous nucleation mechanism should be considered possible on Cu clusters. The only possible process is therefore the reduction of the nucleation barrier of α-Al nanocrystals with Cu addition, as also proposed in Al-Ce-Ni-Cu alloys [60]. Nevertheless, studies regarding the Al primary crystallisation in Al-Sm-Ni-Cu alloys suggest that the addition of Cu induces heterogeneities based upon medium range order that can act as nucleation sites [61]. Similar studies can be found in [62].

3.4. Second crystallisation stage

The second exothermic reaction in the crystallisation process appears in DSC traces with a maximum at approximately 340 °C and with a smaller temperature range than the first one (Figure 3c). A detailed examination also shows a tail at the low temperatures side.

DSC traces in Figure 3 were obtained with a heating rate of 20 °C/min, resulting in the third reaction starting almost before the second one has

finished. In order to achieve a wider separation between both reactions, different heat treatments were tried. It was found that a continuous heat treatment at 20 °C/min up to 25 °C before the second reaction maximum temperature, followed by an isothermal heat treatment, allows to reach the end of the second reaction without immediately initiating the third one. This however appeared a few minutes later (Figure 8). The separation is more efficient for both Cu-containing alloys, with the third reaction more separated from the second one. As expected (because of the aforementioned low temperatures tail), the second reaction appears now divided into two different ones, being clearer for the Cu-free alloy. This is in agreement with the shape found in continuous heat treatments (Figure 3c), where the second subreaction is much clearer in the Cu-free alloy. This somewhat different behaviour could be revealing a possible difference in the crystallisation process, to be discussed in the next sections.

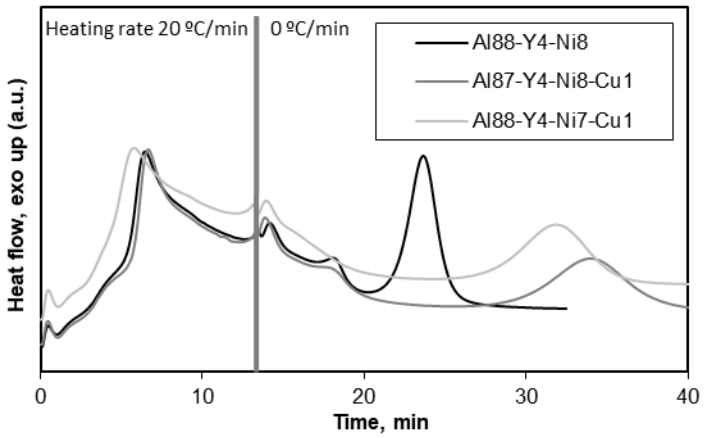

Figure 8. DSC traces of the studied alloys carried out at 20 ºC/min up to 25 °C before the second reaction maximum temperature, followed by an isothermal heat treatment.

XRD patterns corresponding to heat treatments up to the end of the first and the second subreactions of the second crystallisation stage (Figure 9) seem to show that in both cases it is only possible to find α-Al nanocrystals. Similarly, no other diffraction spots are present from other phases after TEM characterization.

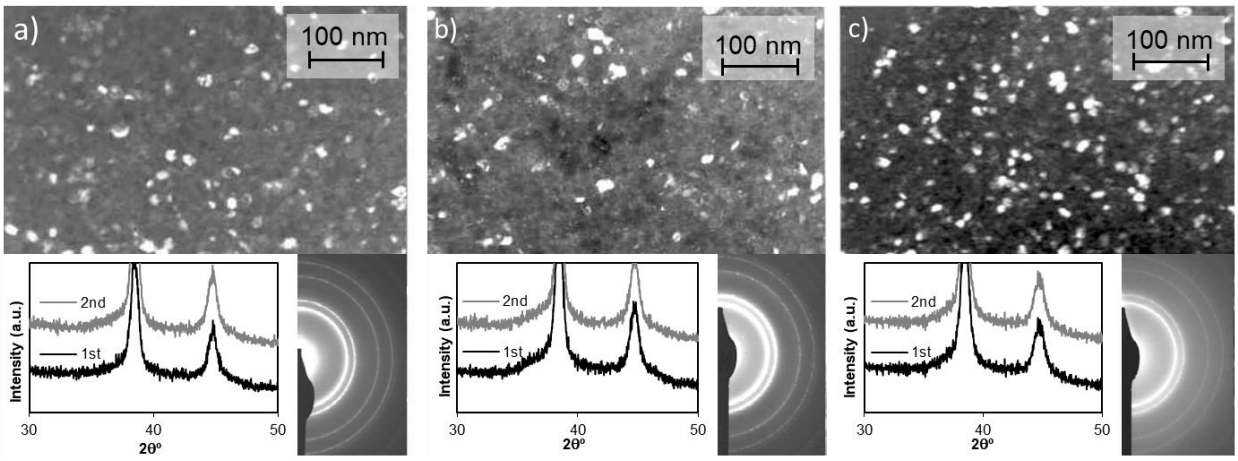

Figure 9. TEM dark field images and DP, and XRD patters of heat treated ribbons up to the end of the second DSC reaction of a) Al_{88}-Y_4-Ni_8, b) Al_{87}-Y_4-Ni_8-Cu_1 and c) Al_{88}-Y_4-Ni_7-Cu_1 alloys. Also XRD patterns after the first DSC subreaction are shown.

Nevertheless, a detailed examination of the XRD patterns on the left side of the main Al peak reveals an asymmetry that cannot be found after the first DSC reaction. New phases should therefore be appearing, probably just nucleating, but to an extent that does not allow their identification. Also, Al nanocrystals growth could contribute to the DSC reactions.

Several researchers have tried to provide an explanation for the process taking place in this second and subsequent crystallisation stages. In the first studies with the alloy Al_{85}-Y_5-Ni_{10} [45, 49-51], results were not totally clear, and only α-Al, Al_3Ni, $Al_{16}YNi_3$ and unidentified phases where indicated to appear. They were, however, not clearly related to the different crystallisation stages, and results mainly referred to the end of the crystallisation process. Several references can be found for the $Al_{16}YNi_3$ phase, however the metastable $Al_{19}Y_3Ni_5$ phase was later proposed to be the real Al-rich phase appearing in the system, and the $Al_{23}Y_4Ni_6$ the equilibrium ternary phase [63, 64], both of them with a very similar structure to Al_4YNi [65, 66].

More recently [67], the crystallisation of an Al_{80}-Y_5-Ni_{15} alloy lead to Al, Al_3Ni and $Al_{23}Y_4Ni_6$, the latter appearing through a peritectic reaction between the amorphous phase and Al_3Ni, initially in a higher amount. Also, after the primary crystallisation of the Al_{85}-Y_4-Ni_{11} alloy, the second and third DSC reactions were detected at 332 ºC and 357 ºC, and also a fourth small reaction at 446 ºC [18]. In this alloy, XRD spectra from a sample heat

treated at 300 ºC for 40 min revealed the presence of Al_3Ni and $Al_{19}Y_3Ni_5$ peaks, suggesting that the controversial second reaction was due both to these phases crystallisation and α-Al growth. The following reactions were related to the disappearance of the metastable ternary and the Al_3Ni phases, and the final crystallisation of Al_9YNi_3. As indicated in the study, small DSC reactions could also be due to morphological changes. It was also pointed out that the equilibrium ternary intermetallic $Al_{23}Y_4Ni_6$ was not found in the spectra, since a true equilibrium state was not reached even after 40 h at 550 ºC. The aforementioned could be in agreement with the enthalpies of formation of intermetallic in the Al-Y-Ni system [28, 64, 68], being lower for $Al_{19}Y_3Ni_5$ than for $Al_{23}Y_4Ni_6$.

Another recent study using in situ synchrotron diffraction on Al_{87}-Y_4-Ni_9 and Al_{86}-Y_4-Ni_{10} [26], revealed a two-stage crystallisation process. The first was related to the crystallisation of f.c.c. α-Al and the second took place after heating above 347 ºC, with the Al_3Ni and $Al_{19}Y_3Ni_5$ phases simultaneously appearing, together with α-Al grain growth, all in agreement with the aforementioned results. At ~700 ºC the sample begins to melt and the partially disordered Al_9YNi_3 appears while α-Al and Al_3Ni phases start disappearing. Increasing Ni content in Al_{83}-Y_4-Ni_{13} results in a third peak being observed, although the sequence is different because of the higher amount of solute, also causing the metastable Al_9Ni_2 phase to appear before α-Al. The second reaction corresponds to the Al_9Ni_2 phase decomposition and Al_3Ni formation, maybe together with a unidentified phase at a very low concentration. The third stage corresponds to the appearance of the $Al_{19}Y_3Ni_5$ phase. When the Ni content in an Al_{75}-Y_{10}-Ni_{15} alloy is further increased, the initially crystallised $Al_{19}Y_3Ni_5$ phase continuously transforms to $Al_{23}Y_4Ni_6$ from temperatures around 600 ºC. The transformations is however reverted when cooling. This denies the metastable character of the $Al_{19}Y_3Ni_5$ phase.

A recently published result [53] deals with the appearance of the ternary alloys when cooling from the liquid phase. It is shown that Y_2O_3 acts as nucleating sites for $Al_{23}Y_4Ni_6$ and then α-Al, although no binary particles such as Al_3Ni were found.

From these studies, it can be inferred that the nucleation of both Al_3Ni and $Al_{19}Y_3Ni_5$ phases could be the cause of the two observed subreactions in the second DSC reaction. In addition, α-Al grains growth should be taking place

from the first DSC reaction. The association of one of the two sub-reactions to the appearance of each of the two intermetallics is something not yet clarified, although the different behaviour in the Cu-free and Cu-containing alloys (Figure 8) could be related with this. This will be discussed after the study of the third DSC reaction.

Although the volume fraction of these two phases in too small to clearly identify them, an estimation of the intermetallics crystallisation process can be done. The activation energy for the formation of intermetallic phases can be assumed to be a 25% higher than that of α-Al nanocrystals [47]. Areas under the DSC curves of about 50 J/g for the first reaction, and 15 and 10 J/g for the two processes of the second reaction were measured. Third, considering that α-Al nuclei about 10 nm in diameter (525 nm^3) have formed in the first reaction with 50 J/g, and assuming a similar number density of intermetallics, particles with diameters of 6.2 and 5.4 nm should be formed in case of homogeneous nucleation and growth of the new intermetallics. However, a layer of 0.37 and 0.25 nm would be formed around existing α-Al nanocrystals. These latter figures would be even smaller if a bigger size is considered for the α-Al nanocrystals. Despite the uncertainties in the previous reasoning, isolated particles should be easier to detect by XRD than very small layers around nanocrystals, therefore the heterogeneous nucleation around existing α-Al nanocrystals being more probable.

3.5. Third crystallisation stage

After heat treating the ribbons beyond the second DSC reaction, the first intermetallics can be clearly found for all the alloys. Figure 10 shows XRD patterns after heat treatments at 20 ºC/min to the maximum temperature of the third DSC reaction, to 375 ºC, held for 30 min., to 450 °C and to 600 °C.

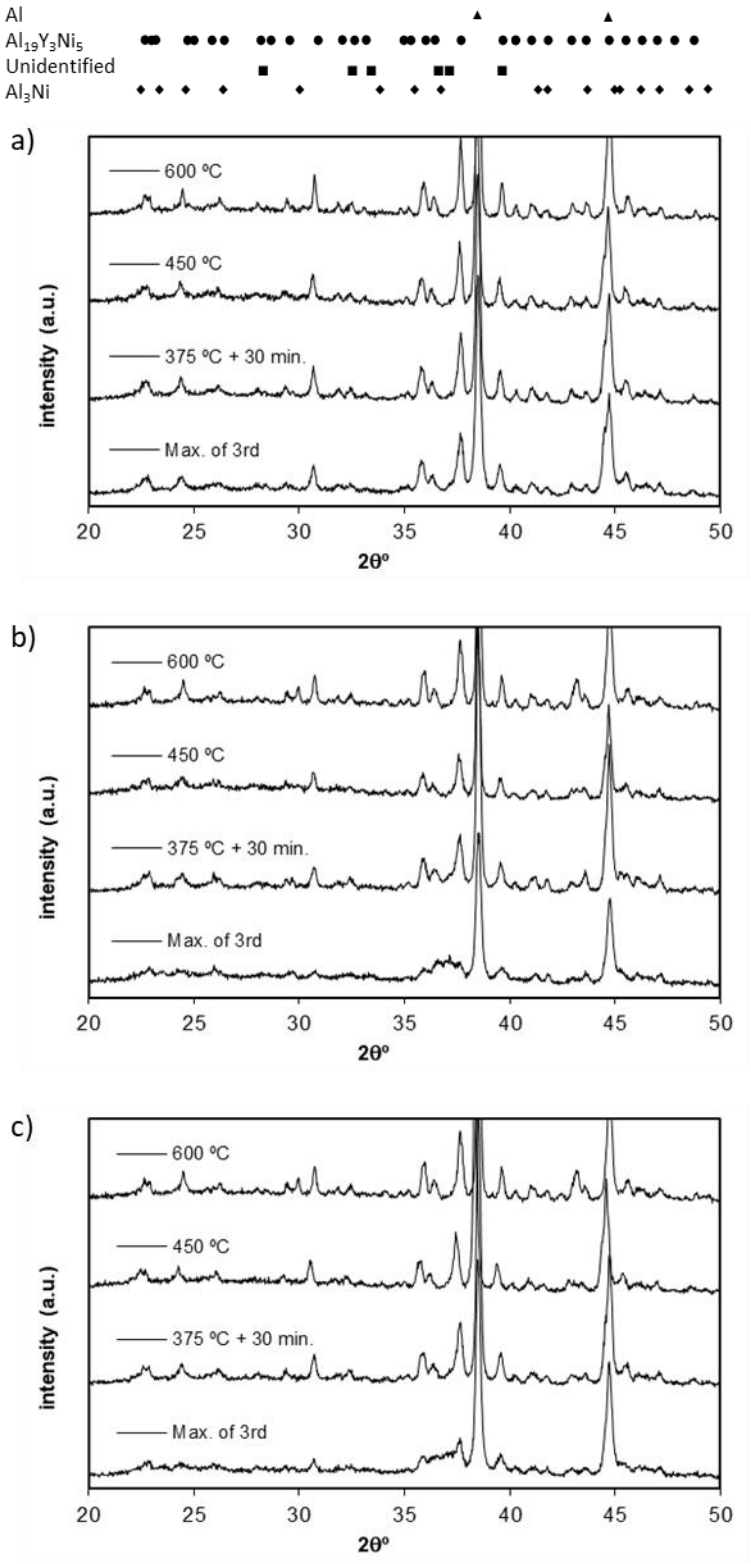

Figure 10. XRD patterns of a) Al_{88}-Y_4-Ni_8, b) Al_{87}-Y_4-Ni_8-Cu_1 and c) Al_{88}-Y_4-Ni_7-Cu_1 alloys, after been heat treated to the maximum of the third DSC reaction, to 375 ºC held for 30 min., to 450 °C and to 600 °C.

Phase identification through XRD peaks positions and intensities after heating to the maximum of the third DSC reaction, reveals the presence of Al, Al-Y-Ni ternary phases, and very probably Al_3Ni. The relatively small amount of Al_3Ni, and peaks position coincidence with those of the ternary phases, make its identification challenging.

In the Cu-free alloy, the ternary phase is identified as $Al_{19}Y_3Ni_5$, being the formation of this phase during the second DSC reaction in agreement with other recent studies [18, 26]. The third DSC reaction must be related to the growth of this phase, an easy process after its nucleation according to the proximity of both reactions (as shown in Figure 3, and clearer in Figure 8).

However, if Cu is present, the situation is not so clear. An unidentified metastable phase appears, with the $Al_{19}Y_3Ni_5$ phase in a clearly lower amount. According to this, the second DSC reaction could now be due to the nucleation of Al_3Ni and the metastable phase. The third reaction should then be responsible for the transformation of the metastable phase and growth of $Al_{19}Y_3Ni_5$. It cannot be discarded that a fraction of the $Al_{19}Y_3Ni_5$ phase directly appears from the amorphous matrix or grows from just formed metastable particles, therefore being much less influenced by this latter phase.

This different behaviour, depending on the Cu presence, could explain the aforementioned differences in the second DSC reaction. The first sub-reaction, similar for the three compositions, could be related to the phase Al_3Ni, whereas the second sub-reaction must depend on the $Al_{19}Y_3Ni_5$ and metastable phases.

Moving on to the results obtained after heating to 375 ºC held for 30 min., with the third reaction in a more advanced state, Al and, very probably, Al_3Ni, were again identified in all the alloys. On the other hand, there is an almost-complete evolution from the unidentified metastable phase to $Al_{19}Y_3Ni_5$ in Cu-containing alloys, which is totally completed at 450 ºC. Therefore, the third DSC reaction is confirmed to be responsible for the transformation of the metastable phase to $Al_{19}Y_3Ni_5$.

Despite recent advances in the knowledge of these crystallisation processes, there are still aspects to clarify. One of them concerns the nature of the aforementioned metastable phase, referenced in studies with Al_{85}-Y_8-Ni_5-

Co_2 [69], appearing without identification in Al_{85}-Ni_7-Y_8 and (Al_{85}-Ni_7-Y_8)$_{98}$-Be_2 [70] and Al_{84}-Y_9-Ni_5-Co_2 [71], or identified as NiY in an (Al_{87}-Ni_5-Y_8)$_{85}$-B_{15} alloy [35]. The only probable conclusion from these studies is the formation of the metastable phase when a certain amount of a fourth element is added to the Al-Y-Ni system. A possible explanation for the nature of this unidentified metastable phase is the modification of the crystalline structure of the stable phase because of the presence of minor alloying elements. In this study, Cu is refused at higher temperatures and the $Al_{19}Y_3Ni_5$ structure appears.

Another unclarified aspect concerns the evolution of the Al_3Ni particles, which according to [67] are supposed to contribute to the ternary phase formation. Figure 11 shows two XRD patterns simulations, as well as the corresponding experimental traces. The first simulation corresponds to the presence of Al, $Al_{19}Y_3Ni_5$ and Al_3Ni in a proportion 75/15/10. Although the presence of the unidentified metastable phase cannot be simulated, by comparing the simulation with the pattern of a Cu-containing alloy after heating to the maximum of the third DSC reaction, the presence of Al_3Ni seems to be verified. The second simulation corresponds to this same alloy after heating to higher temperatures, with Al, $Al_{19}Y_3Ni_5$ and Al_3Ni in proportions 63/35/2. The pattern reassembles the experimental one independently of the presence of Al_3Ni, in a very small amount in the simulation. Although the aforementioned phase proportions are rough figures to reproduce the experimental pattern, and can only be considered qualitatively, it can be concluded that the presence of Al_3Ni decreases with heating, therefore contributing to the formation of the $Al_{19}Y_3Ni_5$ phase.

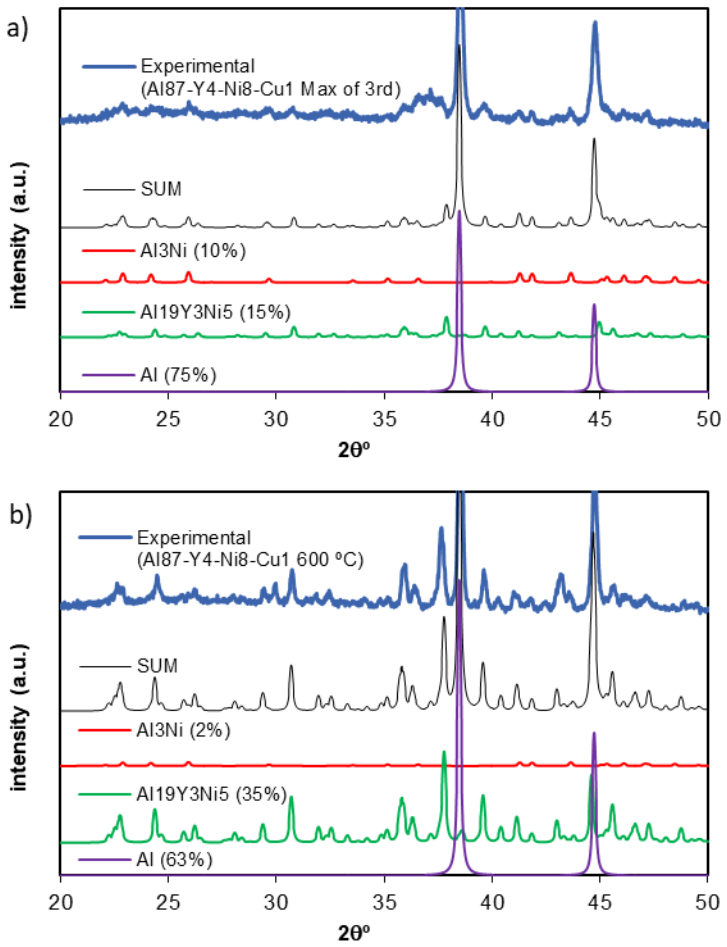

Figure 11. Experimental and simulated XRD patterns of: a) the Al_{87}-Y_4-Ni_8-Cu_1 alloy heat treated to the maximum of the third DSC reaction, and Al-$Al_{19}Y_3Ni_5$-Al_3Ni in proportions 75/15/10 (the metastable phase is not simulated), and b) the Al_{87}-Y_4-Ni_8-Cu_1 alloy heat treated to 600 ºC, and Al-$Al_{19}Y_3Ni_5$-Al_3Ni in proportions 63/35/2.

3.6. Microstructural identification

The microstructural evolution previously analysed by XRD is now completed by TEM, including microdiffraction. Results show that all the studied Al and Al_3Ni particles, now clearly identified, have polygonal or equiaxial shape after any of the studied heat treatments. They will therefore not be considered in the following discussion.

Figure 12 shows the specimens microstructure as observed by TEM after heat treatments to 375 °C held for 30 min. The microstructure consists of

particles with a size smaller than approximately 150 nm and a maximum length in some cases of about 300 nm.

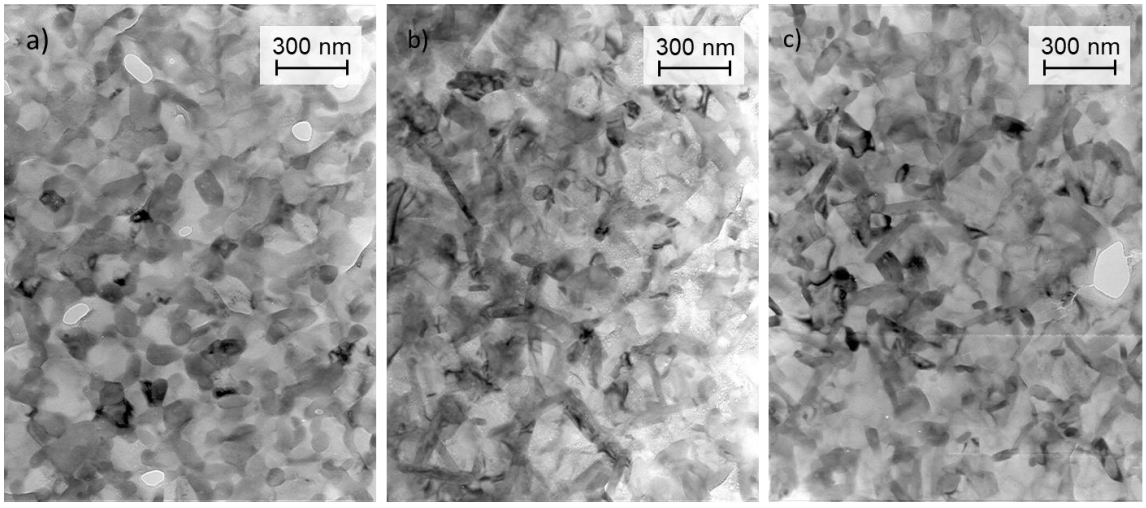

Figure 12. TEM bright field images of heat treated ribbons to 375 ºC held for 30 min. of a) Al_{88}-Y_4-Ni_8, b) Al_{87}-Y_4-Ni_8-Cu_1 and c) Al_{88}-Y_4-Ni_7-Cu_1 alloys.

A slight difference is observed depending on the presence of Cu. In the Cu-free alloy, in which the metastable phase has not been detected, only relatively equiaxial particles are found, therefore the $Al_{19}Y_3Ni_5$ particles must be growing with this shape. For Cu-containing alloys, both equiaxial and slightly elongated particles are found. Thus, the $Al_{19}Y_3Ni_5$ particles (potentially, the only ternary phase present after this treatment) must appear with this elongated shape and/or with equiaxial shape. Assuming that the metastable phase grows with the elongated shape, the stability of this phase in the Cu-containing alloys allows these particles enough time to grow, maintaining this shape once transformed to $Al_{19}Y_3Ni_5$. The stability must be higher in the Al_{87}-Y_4-Ni_8-Cu_1 alloy (as also shown by XRD), in which even some rod-like particles can be observed.

The transformation from the metastable phase to $Al_{19}Y_3Ni_5$ occurs without shape change. Thus, no nucleation process takes place, but just an adjustment of the composition and crystalline structure in the existing particles, possibly having a very similar chemical composition. The rejection of Cu from the unidentified phase to form the $Al_{19}Y_3Ni_5$ phase can then be assumed to occur.

After treatments to 450 ºC (Figure 13), particles sizes remain about 150 nm in diameter, and rods about 40 nm in section and 280 nm long, remaining unchanged after reaching 600 ºC.

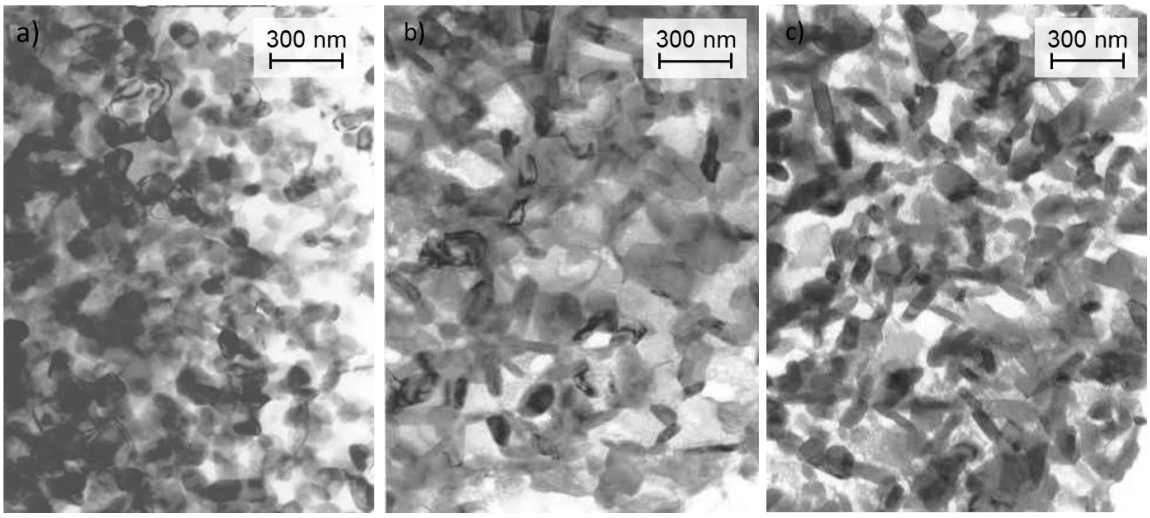

Figure 13. TEM bright field images of heat treated ribbons up to 450 ºC of a) Al_{88}-Y_4-Ni_8, b) Al_{87}-Y_4-Ni_8-Cu_1 and c) Al_{88}-Y_4-Ni_7-Cu_1 alloys.

Previous assumptions regarding the transformation from the unidentified metastable phase to $Al_{19}Y_3Ni_5$ in Cu-containing alloys can be confirmed after TEM microdiffraction on heat treated ribbons to 450 ºC (Figure 14).

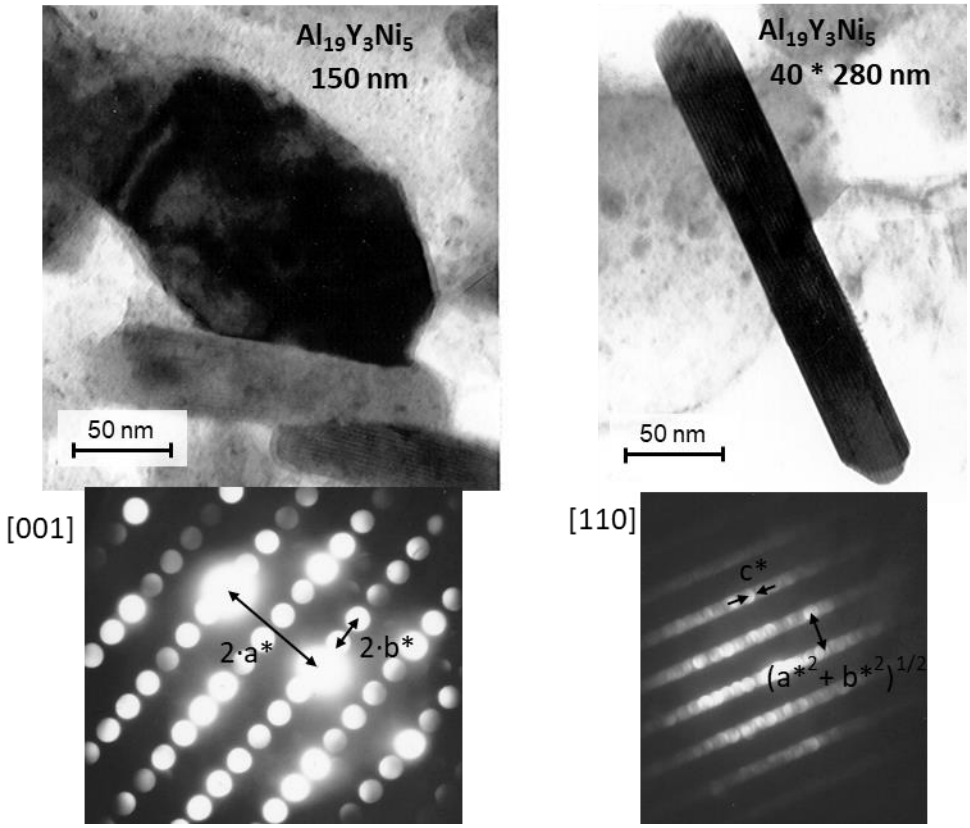

Figure 14. TEM bright field micrographs of selected $Al_{19}Y_3Ni_5$ particles of heat treated ribbons up to 450 ºC, and microdiffraction patterns of an Al_{88}-Y_4-Ni_7-Cu_1 alloy. Reciprocal lattice parameters are indicated in DP.

As shown in Figure 14, the $Al_{19}Y_3Ni_5$ phase for the Cu-containing alloys appears with both equiaxial and rod shapes. This will depend on the history of the particle. If forming from the amorphous matrix after the second DSC reaction or growing from just-formed metastable particles, the equiaxial shape will be found. On the other hand, when appearing after transforming from the metastable phase during the third DSC reaction, the rod shape will be observed.

In summary, Cu seems to be uniformly distributed in the amorphous matrix after primary crystallisation. However, it must be part of the metastable phase appearing when this element is added to the alloy. The identification of $Al_{19}Y_3Ni_5$ both for the Cu-free and Cu-containing alloys after heating to higher temperatures seem to indicate that Cu must be again rejected to the Al matrix. Nevertheless, a residual presence of Cu in the ternary alloy cannot be discarded. Indeed, minor differences are observed in the XRD patterns in the peaks corresponding to this phase related to the presence of Cu (Figure 10).

4. Conclusions.

The addition of 1 at.% Cu to Al_{88}-Y_4-Ni_8 alloy changes the GFA and stability of the amorphous material obtained after melt spinning. Al substitution by Cu increases the stability of the amorphous structure, whereas Ni substitution by Cu decreases it.

Additionally, during the primary crystallisation process, Cu has a clear effect on size reduction of α-Al nanocrystals.

The differences in the primary crystallisation do not seem to affect the crystallisation at higher temperatures, with Al, Al_3Ni, and ternary Al-Y-Ni intermetallic particles always present in the alloy. The ternary phase appears as $Al_{19}Y_3Ni_5$ or as an unidentified metastable structure probably containing Cu but being similar to the former. The presence of Cu stabilizes the metastable phase.

$Al_{19}Y_3Ni_5$ appearing from the amorphous structure grows with equiaxial shape. The metastable phase grows with elongated shape, then directly transforming to $Al_{19}Y_3Ni_5$, which therefore appears with this shape in Cu-containing alloys. Traces of Cu are probably retained in the ternary alloy, slightly modifying its composition.

The addition of Cu could be considered to improve the formation of α-Al, with smaller nanocrystals being formed and better properties expected. However, the presence of elongated intermetallics in Cu-containing alloys will surely degrade the mechanical behaviour after the later stages of crystallisation.

Acknowledgements

The Ministerio de Economía y Competitividad (Spain) and Feder (EU) through the research project DPI2015-69550-C2-2-P are gratefully acknowledged for financial support. The authors also wish to thank Prof. Brian Cantor and Dr. Paul J. Warren for helpful discussion and facilitating the initial experiments carried out at Materials Department of Oxford University.

References

[1] E.D. Zanotto, J.C. Mauro, The glassy state of matter: Its definition and ultimate fate, Journal of Non-Crystalline Solids 471 (2017), 490-495.
[2] J.J. Kruzic, Bulk Metallic Glasses as Structural Materials: A Review, Advanced Engineering Materials 18(8) (2016), 1308-1331.
[3] N.B. Nair, B.G. Priyadarshini, Process, structure, property and applications of metallic glasses, AIMS Materials Science 3(3) (2016), 1022-1053.
[4] H.F. Li, Y.F. Zheng, Recent advances in bulk metallic glasses for biomedical applications, Acta Biomaterialia 36 (2016), 1-20.
[5] J. Yin, H. Cai, X. Cheng, X. Zhang, Al-based bulk metallic glass with large plasticity and ultrahigh strength, Journal of Alloys and Compounds 648 (2015), 276-279.
[6] J. Eckert, J. Das, S. Pauly, C. Duhamel, Mechanical properties of bulk metallic glasses and composites, J. Mater. Res. 22 (2007), 285-301.
[7] J. Schroers, Processing of bulk metallic glass, Adv. Mater. 22 (2010), 1566-1597.
[8] R.O. Suzuki, Y. Komatsu, K.F. Kobayashi, P.H. Shingu, J. Mater. Sci. 18(4) (1983), 1195-1201.
[9] H.S. Chen, C.H. Chen, Structural relaxation in the Al86Mn14 quasicrystal, Phys. Rev. B, 33 (1986), 668-671.
[10] A. Inoue, H.M. Kitamura, T. Masumoto, A.P. Tsai, Y. Bizen, Al-Ge-(Cr or Mn) and Al-Si-(Cr or Mn) quasicrystals with high metalloid concentration prepared by rapid quenching, J. Mater. Sci. Lett. 6 (1987), 771-774.
[11] A.P. Tsai, A. Inoue, T. Masumoto, Ductile Al-Ni-Zr Amorphous Alloys with High Mechanical Strength, J. Mater. Sci. Lett. 7 (1988), 805-807.
[12] Y. He, S.J. Poon, G.J. Shiflet, Synthesis and properties of metallic glasses that contain aluminium, Science, 241 (1988), 1640-1642.
[13] A. Inoue, K. Ohtera, T. Masumoto, New Amorphous Al-Y, Al-La and Al-Ce Alloys Prepared by Melt Spinning, Jpn. J. Appl. Phys., 27 (1988), L736.
[14] A. Inoue, K. Ohtera, A.P. Tsai, T. Masumoto, New Amorphous Alloys with Good Ductility in Al-Y-M and Al-La-M (M=Fe, Co, Ni or Cu) Systems, Jpn. J. Appl. Phys., 27 (1988), L280.
[15] A. Inoue, K. Ohtera, K. Kith, T. Masumoto, New Amorphous Alloys with Good Ductility in Al-Ce-M (M=Nb, Fe, Co, Ni or Cu) Systems, Jpn. J. Appl. Phys., 27 (1988), L1796.
[16] A. Inoue, K. Ohtera, A. P. Tsai, T. Masumoto, Aluminum-Based Amorphous Alloys with Tensile Strength above 980 MPa (100 kg/mm2), Jpn. J. Appl. Phys., 27 (1988), L479

[17] Y.H. Kim, A. Inoue, T. Masumoto, Ultrahigh Mechanical Strengths of Al88Y2Ni10−xMx (M=Mn, Fe or Co) Amorphous Alloys Containing Nanoscale fcc-Al Particles, Mater. Trans., JIM 32 (1991), 599-608.
[18] M.D.H. Lay, A.J. Hill, P.G. Saksida, M.A. Gibson, T.J. Bastow, ^{27}Al NMR measurement of fcc Al configurations in as-quenched Al85Ni11Y4 metallic glass and crystallization kinetics of Al nanocrystals, Acta Materialia 60(1) (2012), 79-88.
[19] D.C. Hofmann, J.-Y. Suh, A. Wiest, G. Duan, M.-L. Lind, M.D. Demetriou, W.L. Johnson, Designing metallic glass matrix composites with high toughness and tensile ductility, Nature 451 (2008) 1085-1089.
[20] Y.H. Kim, A. Inoue, T. Matsumoto, Ultrahigh tensile strengths of Al88Y2Ni9Mi (M=Mn or Fe) amorphous alloys containing finely dispersed fcc-Al particles, Mater. Trans., JIM. 31 (1990), 747-749.
[21] Y.H. Kim, A. Inoue, T. Matsumoto, Increase in Mechanical Strength of Al–Y–Ni Amorphous Alloys by Dispersion of Nanoscale fcc-Al Particles, Mater. Trans., JIM. 32 (1991), 331-338.
[22] Z.C. Zhong, X.Y. Jiang, A.L. Greer, Micro structure and hardening of Al-based nanophase composites, Mater. Sci. Eng. A 226–228 (1997), 531-535.
[23] H.S Kim, P.J. Warren, B. Cantor, H.R. Lee, Mechanical properties of partially crystallized aluminium based amorphous alloys, NanoStructured Materials 11(2) (1999), 241-247.
[24] G.E. Abrosimova, A.S. Aronin, I.I. Zver'kova, Y.V. Kir'yanov, Phase transformations upon crystallization of amorphous Al-Ni-RE alloys, Physics of Metals and Metallography 94(1) (2002) 102-107.
[25] Y.K. Kim, J.R. Soh, D.K. Kim, H.M. Lee, Glass formation in metallic Al-Ni-Y, Journal of Non-Crystalline Solids 242 (1998), 122-130.
[26] M.J. Styles, W.W. Sun, D.R. East, J.A. Kimpton, M.A. Gibson, C.R. Hutchinson, On the competition in phase formation during the crystallisation of Al-Ni-Y metallic glasses, Acta Materialia 117 (2016), 170-187.
[27] Y. Shen, J.H. Perepezko, Al-based amorphous alloys: Glass-forming ability, crystallization behavior and effects of minor alloying additions, Journal of Alloys and Compounds 707 (2017), 3-11,
[28] S.P. Sun, D.Q. Yi, H.Q. Liu, B. Zang, Y. Jiang, Calculation of glass forming ranges in Al–Ni–RE (Ce, La, Y) ternary alloys and their sub-binaries based on Miedema's model, Journal of Alloys and Compounds 506 (2010), 377-387.
[29] M.F. de Oliveira, L.C.R. Aliaga, C. Bolfarini, W.J. Botta, C.S. Kiminami, Thermodynamic and topological instability approaches for

forecasting glass-forming ability in the ternary Al-Ni-Y system, Journal of Alloys and Compounds 464(1-2) (2008) 118-121.
[30] Z. Zhang, X.Z. Xiong, W. Zhou, X. Lin, A. Inoue, J.F. Li, Glass forming ability and crystallization behavior of Al–Ni–RE metallic glasses, Intermetallics 42 (2013) 23-31.
[31] Q. Wang, J.H. Li, J.B. Liu, B.X. Liu, Atomistic Design of Favored Compositions for Synthesizing the Al-Ni-Y Metallic Glasses, Scientific Reports 5 (2015), 16218
[32] M. Yewondwossen, R.A Dunlap, D.J. Lloyd, Thermal and electronic properties of amorphous Al87Y8Ni5-xTMx (TM=Mn, Fe, CO, Cu), J. Phys Condens. Matter 4 (1992), 461-472.
[33] S.J. Hong, P.J. Warren, B.S. Chun, Nanocrystallization behaviour of Al–Y–Ni with Cu additions, Materials Science and Engineering A 304-306 (2001), 362-366.
[34] P.J. Squire, I.T.H. Chang, Development of rapidly solidified Al–Y–Ni-based alloys, Materials Science and Engineering A 449-451 (2007), 1009-1012.
[35] S.-F. Chen, C.-Y. Chen, C.-H. Lin, Insight on the glass-forming ability of Al-Y-Ni-Ce bulk metallic glass, Journal of Alloys and Compounds 637 (2015), 418-425.
[36] M. Gögebakan, The Effect of Si Addition on Crystallization Behavior of Amorphous Al-Y-Ni Alloy, J. of Mater. Eng. and Perform. 13 (2004), 504-508.
[37] S.-F Chen, J.-K. Chen, S.-L. Lin, Y.-L. Lin, Effects of B upon glass forming ability of Al87Y8Ni5 amorphous alloy, Journal of Alloys and Compounds 565 (2013), 29-36.
[38] J.-H. Jun, J.-M. Kim, K.-T. Kim, W.-J. Jung, Glass formability and thermal stability of Al–Ni–Y–Be amorphous alloys, Journal of Alloys and Compounds 434-435 (2007), 190-193.
[39] J. Latuch, A. Kokoszkiewicz, H. Matyja, The Effect of Cu Addition on the Formation of fcc-Al Phase in Rapidly Quenched Al-Y-Ni Alloys, Mater. Sci. Eng. A 226-228 (1997), 809-812.
[40] Y. Li, S. Zhao, Y. Liu, P. Gong, J. Schroers, How Many Bulk Metallic Glasses Are There?, ACS Comb. Sci. 19(11) (2017), 687-693.
[41] S. Kuthe, A. Deshmukh, U. Palikundwar, J. Bhatt, Computational Platform for Manufacturing Bulk Metallic Glasses Based on GFA Parameters, Transactions of the Indian Institute of Metals 71(11) (2018), 2731-2734.

[42] Z.P. Chen, J.E. Gao, Y. Wu, H. Wang, X.J. Liu, Z.P. Lu, Designing novel bulk metallic glass composites with a high aluminum content, Scientific Reports 3 (2013), 3353.
[43] R.S. Maurya, A. Sahu, T. Laha, Quantitative phase analysis in Al86Ni8Y6 bulk glassy alloy synthesized by consolidating mechanically alloyed amorphous powder via spark plasma sintering, Materials and Design 93 (2016), 96-103.
[44] R.S. Maurya, A. Sahu, T. Laha, Effect of consolidation pressure on phase evolution during sintering of mechanically alloyed Al86Ni8Y6 amorphous powders via spark plasma sintering, Materials Science and Engineering A 649 (2016), 48-56.
[45] W.T. Kim, M. Gogebakan, B. Cantor, Heat treatment of amorphous Al85Y5Ni10 and Al85Y10Ni5 alloys, Materials Science and Engineering A 226-228 (1997), 178-182.
[46] K.K. Sahu, N.A. Mauro, L. Longstreth-Spoor, D. Saha, Z. Nussinov, M.K. Miller, K.F. Kelton, Phase separation mediated devitrification of Al88Y7Fe5 glasses, Acta Materialia 58(12) (2010), 4199-4206.
[47] Z.H. Huang, J.F. Li, Q.L. Rao, Y.H. Zhou, Primary crystallization of Al–Ni–RE amorphous alloys with different type and content of RE, Materials Science and Engineering A 489(1–2) (2008), 380-388.
[48] C. Chattopadhyay, B.S. Murty, Kinetic modification of the ‘confusion principle’ for metallic glass formation, Scripta Materialia 116 (2016), 7-10.
[49] J. Latuch, H. Matyja, V.I. Fadeeva, Crystallization of amorphous A185Y10Ni 5 and A185YsNi10 alloys, Materials Science and Engineering, A 179-180 (1994), 506-510.
[50] S. Saini, A. Zaluska, Z. Altounian, Effect of glass short-range order on crystallization onset in Al-Y-Ni glasses, Journal of Non-Crystalline Solids 250-252 (1999), 714-718.
[51] B.C. Ko, Y.C. Yoo, High temperature deformation behavior of Al85Ni10Y5 alloy produced by hot extrusion using an amorphous ribbon, Journal of Materials Science Letters 18 (1999), 1765-1768.
[52] R. Jindal, V.S. Raja, M.A. Gibson, M.J. Styles, T.J. Bastow, C.R. Hutchinson, Effect of annealing below the crystallization temperature on the corrosion behavior of Al–Ni–Y metallic glasses, Corrosion Science 84 (2014), 54-65.
[53] A. Kuball, M. Stolpe, R. Busch, Crystallization behavior of the Al86Ni8Y6 metallic glass forming alloy upon rapid cooling, Journal of Alloys and Compounds 737 (2018), 398-404.

[54] B. Cao, S. Li, D. Yi, Study on the crystallization of Al88.5Y6.5Ni5 (at.%) amorphous alloy, Journal of the Less-Common Metals 171 (1991), l-8.
[55] M. Gogebakan, P.J. Warren, B. Cantor, Crystallization behaviour of amorphous Al85Y11Ni4 alloy, Materials Science and Engineering A 226-228 (1997), 168-172.
[56] E. Pershina, D. Matveev, G. Abrosimova, A. Aronin, Formation of nanocrystals in an amorphous Al90Y10 alloy, Materials Characterization 133 (2017), 87-93.
[57] T. Egami, Y. Waseda, Atomic size effect on the formability of metallic glasses, J. Non-Cryst. Solids 64 (1984), 113-134.
[58] X.Y. Jiang, Z.C. Zhong, A.L. Greer, Particle-size effects in primary crystallization of amorphous Al-Ni-Y alloys, Materials Science and Engineering A 226-228 (1997) 789-793.
[59] T. Gheiratmand, H.R. Madaah Hosseini, Finemet nanocrystalline soft magnetic alloy: Investigation of glass forming ability, crystallization mechanism, production techniques, magnetic softness and the effect of replacing the main constituents by other elements, Journal of Magnetism and Magnetic Materials 408 (2016), 177-192.
[60] K. Hono, Y. Zhang, A. Inoue, T. Sakurai, Atom Probe Studies of Nanocrystalline Microstructural Evolution in Some Amorphous Alloys, Mater. Trans., JIM 36 (1995), 909-917.
[61] J.H. Perepezko, S.D. Imhoff, R.J. Hebert, Nanostructure development during devitrification and deformation, Journal of Alloys and Compounds 495 (2010), 360-364.
[62] D.H. Kim, W.T. Kim, E.S. Park, N. Mattern, J.Eckert, Phase separation in metallic glasses, Progress in Materials Science 58(8) (2013), 1103-1172.
[63] R. Raggio, G. Borzone, R. Ferro, The Al-rich region in the Y-Ni-Al system: microstructures and phase equilibria, Intermetallics 8 (2000), 247-257.
[64] A.L. Vasiliev, M. Aindow, M.J. Blackburn, T.J. Watson, Phase Stability and Microstructure in Devitrified Al-Rich Al-Y-Ni Alloys, Intermetallics 12 (2004), 349-362.
[65] W.J. Golumbfskie, R. Arroyave, D. Shin, Z.-K. Liu, Finite-temperature thermodynamic and vibrational properties of Al–Ni–Y compounds via first-principles calculations, Acta Materialia 54 (2006) 2291-2304.
[66] D. Shin, W.J. Golumbfskie, E.R. Ryba, Z.-K. Liu, First-principles study of Al–Ni–Y ternary compounds for crystal structure validation, J Alloys Comp 462 (2008) 262-266.

[67] S. Mudry, Yu. Kulyk, V. Mykhaylyuk, B. Tsizh, Structure changes in Al80Ni15Y5 amorphous alloy, J Non-Crystalline Solids 354 (2008) 4488-4490.
[68] W.J. Golumbfskie, S.N. Prins, T.J. Eden, Z.-K. Liu, Predictions of the Al-rich region of the Al–Co–Ni–Y system based upon first-principles and experimental data, CALPHAD 33 (2009), 124-135.
[69] D.V. Louzguine, A. Inoue, Influence of a supercooled liquid on crystallization behaviour of Al–Y–Ni–Co metallic glass, Materials Letters 54 (2002), 75-80.
[70] J.-H. Jun, J.-M. Kim, K.-T. Kim, W.-J. Jung, Glass formability and thermal stability of Al–Ni–Y–Be amorphous alloys, Journal of Alloys and Compounds 434–435 (2007), 190–193.
[71] N. Bassim, C.S. Kiminami, M.J. Kaufman, M.F. Oliveira, M.N.R.V. Perdigao, W.J. Botta Filho, Crystallization behavior of amorphous Al84Y9Ni5Co2 alloy, Materials Science and Engineering A 304–306 (2001), 332–337.